BIOCHEMISTRY
including biophysical chemistry & molecular biology
Article

Heme Pocket Structural Properties of a Bacterial Truncated Hemoglobin from *Thermobifida fusca*[†]

Enrica Droghetti,[‡] Francesco Paolo Nicoletti,[‡] Alessandra Bonamore,[§] Leonardo Boechi,[‖] Pau Arroyo Mañez,[‖] Dario A. Estrin,[‖] Alberto Boffi,[§] Giulietta Smulevich,[‡] and Alessandro Feis*,[‡]

[‡]*Dipartimento di Chimica "Ugo Schiff", Università di Firenze, Via della Lastruccia 3, I-50019 Sesto Fiorentino (FI), Italy,* [§]*Institute Pasteur, Fondazione Cenci Bolognetti, Department of Biochemical Sciences and CNR Institute of Molecular Biology and Pathology, University of Rome "La Sapienza", Piazzale Aldo Moro 5, I-00185 Rome, Italy, and* [‖]*Departamento de Química Inorgánica, Analítica y Química Física/INQUIMAE-CONICET, Facultad de Ciencias Exactas y Naturales, Universidad de Buenos Aires, Ciudad Universitaria, Pabellón II (C1428EHA), Buenos Aires, Argentina*

ABSTRACT: An acidic surface variant (ASV) of the "truncated" hemoglobin from *Thermobifida fusca* was designed with the aim of creating a versatile globin scaffold endowed with thermostability and a high level of recombinant expression in its soluble form while keeping the active site unmodified. This engineered protein was obtained by mutating the surface-exposed residues Phe107 and Arg91 to Glu. Molecular dynamics simulations showed that the mutated residues remain solvent-exposed, not affecting the overall protein structure. Thus, the ASV was used in a combinatorial mutagenesis of the distal heme pocket residues in which one, two, or three of the conserved polar residues [TyrB10(54), TyrCD1(67), and TrpG8(119)] were substituted with Phe. Mutants were characterized by infrared and resonance Raman spectroscopy and compared with the wild-type protein. Similar Fe−proximal His stretching frequencies suggest that none of the mutations alters the proximal side of the heme cavity. Two conformers were observed in the spectra of the CO complexes of both wild-type and ASV protein: form 1 with ν(FeC) and ν(CO) at 509 and 1938 cm^{-1} and form 2 with ν(FeC) and ν(CO) at 518 and 1920 cm^{-1}, respectively. Molecular dynamics simulations were performed for the wild-type and ASV forms, as well as for the TyrB10 mutant. The spectroscopic and computational results demonstrate that CO interacts with TrpG8 in form 1 and interacts with both TrpG8 and TyrCD1 in form 2. TyrB10 does not directly interact with the bound CO.

Truncated hemoglobins (trHb's)[1] make up a family of small oxygen-binding proteins that are widely distributed among bacteria, protozoa, and plants (*1*, *2*). Their amino acid sequence is 20−40 residues shorter than that of animal hemoglobins, because they lack two of the eight helices typical of the globin fold. They are characterized by a typical structural fold with a two-over-two helical structure, and by a remarkable variability in the nature of the amino acid residues within the heme active site (*3*). Therefore, trHb's have been assigned to a distinct group within the globin superfamily and further divided, on the basis of phylogenetic analysis, into three groups that share less than 30% sequence similarity with each other (*1*, *4*). Group II is the most populated of the three and is characterized by the presence of a Trp residue (G8 position) in the heme distal pocket. The crystal structures of group II trHb's from *Bacillus subtilis* (Bs-trHb) (*5*), *Thermobifida fusca* (Tf-trHb) (*6*), *Geobacillus stearothermophilus* (Gs-trHb) (*7*), and *Mycobacterium tuberculosis* (Mt-trHbO) (*8*) revealed a common pattern of the heme pocket, characterized by an ensemble of polar residues in contact with the iron-bound

ligand coordination shell, which has been defined as a "ligand-inclusive hydrogen bond network" (*9*). In Bs-trHb and Gs-trHb, the H-bond network involves the hydroxyl of TyrB10, the amide group of GlnE11, and the nitrogen atom of TrpG8. A prevalent role of TrpG8 has been demonstrated in spectroscopic and computational studies of Bs-trHb (*10*, *11*).

In both Tf-trHb and Mt-trHbO, the E11 position is a Leu residue, and an additional potential H-bond donor is the TyrCD1 residue (see Figure 1). Therefore, there are three potential H-bond donors in the distal cavity of all class II bacterial trHb's. Identifying the residues that actually interact with the Fe-bound ligand is not a simple task. The first approach consists of tracing the residues that can interact with the ligand on the basis of the interatomic distances as determined by X-ray crystallography. This must be followed by measurements on the "working" protein, namely, by steady-state and/or dynamic spectroscopy on ligand-bound proteins in solution. Among these techniques, the combination of resonance Raman (RR) and infrared spectroscopy of the CO-ligated forms has been successfully employed in characterizing the active site of heme proteins (*12*, *13*). In fact, when data are available for the wild-type protein and distal mutants, the vibrational frequencies can be reliably related to specific interactions between the iron-bound CO and the distal residues. In the past few years, computer simulation techniques have been shown to be very useful in providing microscopic detail about the dynamics of the active site of heme proteins, particularly in the case of trHb's (*10*, *14−18*).

*To whom correspondence should be addressed. Phone: +39 055 457 3088. Fax: +39 055 457 3077. E-mail: alessandro.feis@unifi.it.
[1]Abbreviations: trHb, truncated hemoglobin; ASV, acidic surface variant; WT, wild type; Tf, *Thermobifida fusca*; Mt, *Mycobacterium tuberculosis*; Gs, *Geobacillus stearothermophilus*; Bs, *Bacillus subtilis*; RR, resonance Raman; MD, molecular dynamics; PDB, Protein Data Bank.
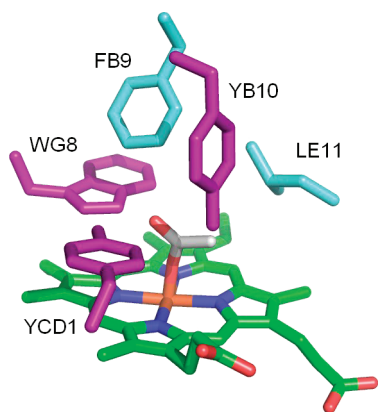
FIGURE 1: Close-up view of the distal side of Tf-trHb. The relevant residues that can interact with the iron-bound ligand (acetate) are colored purple. The distal side is completed by a Phe and a Leu residue (cyan). Data from PDB entry 2BMM (6), relative to the ferric acetate adduct of the protein. The picture was created with PyMol (DeLano Scientific).

The aim of this work is to single out the contributions of the active site hydrogen bonding triad TyrB10, TyrCD1, and TrpG8 by "isosteric permutations" with Phe side chains. Such a small scale combinatorial mutagenesis approach has not been systematically applied to globins but has been performed in this study up to the generation of a triple mutant in which polar interactions with the iron-bound ligand are completely abolished. The mutagenesis study has been conveniently conducted with an acidic surface variant (ASV) of the protein in which surface-exposed residues Phe107 and Arg91 have been mutated to glutamic acid to increase protein solubility. The interpretation of our experimental data has been corroborated by molecular dynamics (MD) simulations of both the wild type and a singly mutated protein. The agreement of experimental and computational studies yields a very detailed understanding of the dynamics of the active site of this protein.

EXPERIMENTAL PROCEDURES

Genetic Engineering Procedures. Tf-trHb was expressed as a recombinant protein in *Escherichia coli* cells and purified as described previously (6). All mutants were obtained by PCR on plasmid pET28b-trtfHb as a DNA template. Site-directed mutagenesis was conducted with the Quikchange mutagenesis kit (Stratagene, La Jolla, CA) according to the manufacturer's instructions, using complementary oligonucleotide pairs introducing the amino acid substitutions. The mutants were transformed into *E. coli* XL1 Blue competent cells, selected on kanamycin plates, and screened by DNA sequencing. Plasmid DNA bearing the gene with the desired mutation was then transformed into *E. coli* BL21(DE3) cells (Novagen) for expression. The mutated proteins were extracted and purified according to the same procedure used for the WT protein.

Sample Preparation. All measurements were performed at room temperature in a 0.1 M buffer solution at pH 7.0. The ferrous forms were obtained via addition of a freshly prepared sodium dithionite (Fluka Chemicals) solution to the deoxygenated fresh protein solution to a final concentration of 3 mM. Because Tf-trHb displays a high affinity for sulfide (19), all experiments were conducted with the smallest amount of reducing agent to avoid the formation of a stable low-spin ferric sulfide adduct. CO complexes were prepared via equilibration of 30 μM (Raman) or 3 mM (infrared) protein solutions with 1 atm

of ^{12}CO (Rivoira) or ^{13}CO (FluoroChem) and finally addition of dithionite to a final concentration of 3 mM (Raman) or 10 mM (infrared).

Spectroscopic Characterization. Electronic absorption spectra, measured with a double-beam spectrophotometer (Varian Cary 5), were recorded both before and after the RR measurements. No sample degradation was observed under the experimental conditions employed. RR spectra were recorded with 413.1 nm (Kr$^+$ laser, Coherent, Innova 300C) and 441.6 nm (He−Cd laser, Kimmon IK4121R-G) excitation using a triple spectrometer (consisting of two Acton Research SpectraPro 2300i instruments working in the subtractive mode and a SpectraPro 2500i instrument in the final stage), equipped with a liquid nitrogen-cooled CCD detector (Roper Scientific Princeton Instruments). All RR measurements were repeated several times under the same conditions to ensure reproducibility. To improve the signal-to-noise ratio, a number of spectra were accumulated and summed only if no spectral differences were noted. The RR spectra were calibrated with indene, acetone, acetonitrile, and carbon tetrachloride as standards to an accuracy of 1 cm^{-1} for intense isolated bands.

FTIR spectra were recorded on a MAGNA 760 Nicolet spectrometer equipped with an MCT detector. The spectra were recorded in a CaF$_2$ cell with a 50 μm Teflon spacer; 512 scans at 2 cm^{-1} resolution were averaged. The spectra of the ferric, ligand-free proteins measured under the same experimental conditions were subtracted from the spectra of the CO derivative to yield a flat baseline.

Molecular Dynamics. Classical MD were performed starting from the crystal structure of Tf-trHb (6). Because the protein was crystallized in the ferric acetate-bound form, we replaced the acetate ligand with CO. The system was immersed in an octahedral box of 4825 water molecules (20). We used periodic boundary conditions and Ewald sums for treating long-range electrostatic interactions. The SHAKE algorithm (21) was used to keep bonds involving H atoms at their equilibrium length. This allowed us to use a 2 fs time step for the integration of Newton's equations. The parm99 and TIP3P force fields implemented in AMBER were used to describe the protein and water, respectively (22). The histidine tautomeric state and protonation (N$_\varepsilon$-H, N$_\delta$-H, His$^+$) were carefully analyzed for each of the four His residues and set to favor the hydrogen bond network suggested by the experimental crystal structure. No ions were added to the system. All systems were minimized and heated slowly from 0 to 300 K over 200 ps under constant volume conditions to optimize any possible structural clashes. Subsequently, a short simulation at a constant temperature of 300 K, under a constant pressure of 1 bar, was performed for an additional 500 ps to allow the systems to reach proper density using a time step of 0.1 fs. These equilibrated structures were the starting point for 50 ns MD simulations at 300 K. We introduced mutations in silico by changing the corresponding amino acid in the original structure and allowing the system to equilibrate as mentioned earlier.

Hazardous Procedures. Manipulation of CO requires all precautions must be taken for both flammable and highly toxic gases.

RESULTS

The ASV of Tf-trHb differs from the wild-type (WT) protein because both Phe107 and Arg91 are mutated to glutamic acid to increase protein solubility during recombinant expression, without affecting thermostability or ligand binding properties.

The underlying strategy was to modify hydrophobic or positively charged groups on the protein surface to acidic amino acid side chains, endowed with higher solvation enthalpy and hence higher water solubility. The residues chosen for acidic mutation were chosen on the basis of the following criteria. (i) Residues must be hydrophobic or positively charged and surface-exposed. (ii) Residues must not be conserved in structural alignments with other group II globins. (iii) Residues must be distant from the heme entrance cavity. Four amino acid residues were found to conform to these criteria, and a set of single to quadruple mutants was screened for soluble expression by sodium dodecyl sulfate−polyacrylamide gel electrophoresis (SDS−PAGE) (Figure S1 of the Supporting Information). The best performing ASV mutant was the double mutant (Phe107 → Glu and Arg91 → Glu). These mutations did not alter oxygen or CO binding properties or the temperature melting of the protein (data not shown), and the spectroscopic features were almost identical to those of the WT protein. Moreover, MD simulations (see below) show that the Phe107 and Arg91 residues of the WT protein are exposed to the solvent, in a manner similar to that of the corresponding residues of the ASV, Glu107 and Glu91, respectively. This means that the protein overall structure is not affected by the mutation. Therefore, ASV can be taken as an engineered scaffold of the WT protein with improved solubility properties for subsequent site-directed mutagenesis studies on the relevant residues of the distal heme pocket. In particular, our study includes the single, double, and triple mutants in which the polar distal amino acids [TyrB10(54), TyrCD1(67), and TrpG8(119)] have been replaced with Phe residues. Seven variants have been obtained, namely, TrpG8 → Phe (hereafter WG8F), TyrCD1 → Phe (YCD1F), TyrB10 → Phe (YB10F), TyrB10-TrpG8 → Phe (YB10F-WG8F), TyrCD1-TrpG8 → Phe (YCD1F-WG8F), TyrB10-TyrCD1→Phe (YB10F-YCD1F), and TyrB10-TyrCD1-TrpG8 → Phe (YB10F-YCD1F-WG8F).

RR Spectra of the Ligand-Free Ferrous Forms. Ferrous WT Tf-trHb and mutated proteins at pH 7.0 display broad electronic absorption bands with maxima at 428−431 and 558 nm, which are typical of a five-coordinate, high-spin (5c HS) heme (Figure S2 of the Supporting Information).

Consistently, the RR spectra in the high-frequency region show core size marker bands typical of 5c HS forms (ν_3 at 1470 cm^{-1}, ν_{38} at 1524 cm^{-1}, ν_{11} at 1547 cm^{-1}, ν_2 at 1560 cm^{-1}, ν_{37} at 1580 cm^{-1}, and ν_{10} at 1605 cm^{-1}) (data not shown). Therefore, the low-frequency region of the RR spectra yields information about the Fe−proximal His bond strength via the frequency of the corresponding ν(Fe−His) stretching mode, which is active only in the ferrous 5c HS species upon excitation of the Soret absorption band (*23−25*).

Figure 2 compares the low-frequency RR spectra of ferrous Tf-trHb and its mutated variants, obtained with Soret excitation. The spectra indicate the presence of a distorted heme because the 323 cm^{-1} (γ_6) out-of-plane mode is activated. This mode lacks an enhancement mechanism in D_{4h} symmetry but becomes active if the porphyrin undergoes an out-of-plane distortion (*26*). Moreover, according to the assignment obtained for myoglobin (*27*), the weak bands at 374 and 383 cm^{-1} are assigned to bending modes of the propionyl groups. The relative intensity of the propionyl bending bands is reversed in the spectra of most distal mutants.

The band at 411 cm^{-1} is assigned to the bending modes of the vinyl groups. This value is 6 cm^{-1} higher than the corresponding value of horse deoxymyoglobin (*27*), in agreement with the
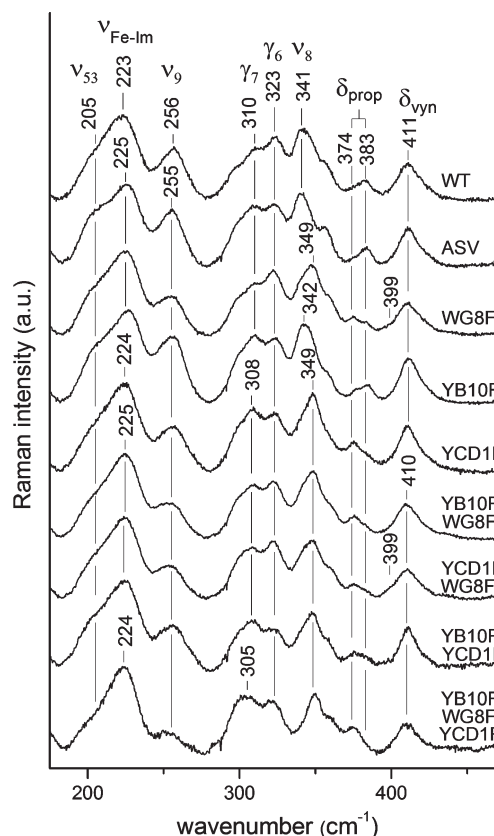

FIGURE 2: RR spectra of native and mutated ferrous Tf-trHb, obtained with an excitation wavelength of 441.6 nm. Experimental conditions: 1 cm^{-1} resolution, 12 mW laser power at the sample, and 320 min total accumulation time (WT); 10 mW laser power at the sample and 120 min (ASV), 210 min (WG8F), 120 min (YCD1F), 120 min (YB10F-WG8F), 210 min (YCD1F-WG8F), 450 min (YB10F-YCD1F), and 70 min (YB10F-YCD1F-WG8F) total accumulation times. Spectra have been shifted along the ordinate axis to allow better visualization.

relatively high frequency of the ν(C=C) stretching mode [1628 cm^{-1} (data not shown)] (*28*).

Finally, we assign the intense band at 223 cm^{-1} to the ν(Fe−His) stretching mode on the basis of the similarity to HbO and HbN (*29, 30*). The frequency is slightly higher (1−2 cm^{-1}) in the spectra of ASV and the other mutated variants.

RR Spectra of the CO-Bound Forms. The UV−visible absorption spectra (with Soret, α, and β bands in the intervals of 420−422, 539−543, and 567−570 nm, respectively) and the high-frequency RR spectra obtained with 413.1 nm excitation (data not shown) are characteristic of six-coordinate low-spin forms, with CO bound as the sixth ligand of the iron atom.

(*i*) *WT and ASV.* Two isotope-sensitive peaks can be detected in the low-frequency region of the RR spectra of the WT Tf-trHb−CO complex (Figure 3A), namely, the bands at 509 and 518 cm^{-1}. They are assigned to ν(FeC) stretching modes. Accordingly, two bands in the region of the bound CO, ν(CO) stretching modes can be identified at 1938 and 1920 cm^{-1}. These bands are detected both in the infrared spectra (Figure 3B) and in the high-frequency region of the RR spectra (Figure S3 of the Supporting Information). Table 1 lists the frequencies that are sensitive to ^{13}CO substitution in the RR spectra, and the corresponding isotopic shifts for the WT as well as for the mutated proteins. On the basis of the correlation between ν(FeC) and ν(CO) frequencies (see Discussion), the spectra allow identification of two conformers that are characterized by ν(FeC)
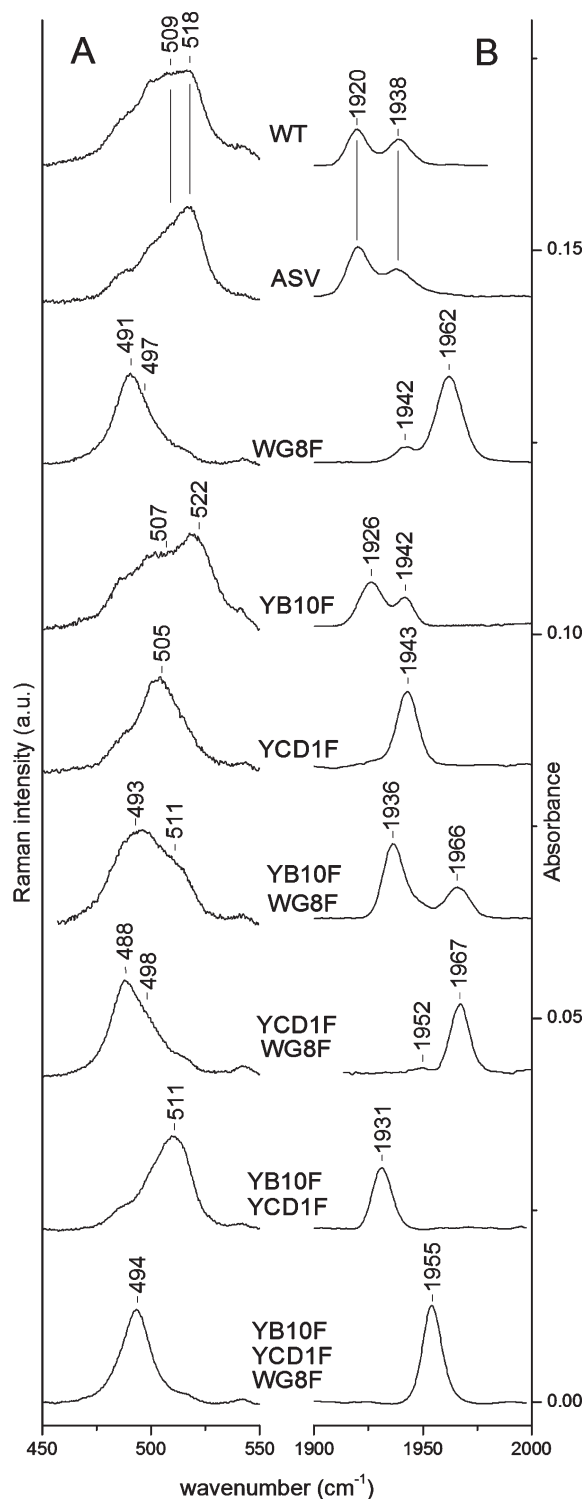
FIGURE 3: RR spectra (left) obtained with an excitation wavelength of 413.1 nm and IR spectra (right) of the CO complexes of native and mutated ferrous Tf-trHb variants at pH 7.0. RR experimental conditions: 1 cm^{-1} resolution for all samples and 10 mW laser power at the sample and 150 min integration time (WT), 4 mW and 105 min (ASV), 5 mW and 120 min (WG8F), 0.5 mW and 640 min (YB10F), 2 mW and 130 min (YCD1F), 2 mW and 60 min (YB10F-WG8F), 15 mW and 120 min (YCD1F-WG8F), 10 mW and 120 min (YB10F-YCD1F), and 15 mW and 60 min (YB10F-YCD1F-WG8F). Spectra have been shifted along the ordinate axis to allow better visualization.

stretching bands at 509 and 518 cm^{-1} and v(CO) stretching bands at 1938 and 1920 cm^{-1}. A change in the relative intensity of these bands is observed for the ASV, the bands at 518 and 1920 cm^{-1} becoming more intense.

Table 1: Vibrational Frequencies (cm^{-1}) of the CO Complexes of WT, the ASV, and Mutated Tf-trHb

	v(FeC), RR[a]	v(CO), IR	v(CO), RR[a]
WT, form 1	509 (504)	1938	1940 (1893)
WT, form 2	518 (514)	1920	1920 (1878)
ASV, form 1	509 (504)	1938	1940 (1893)
ASV, form 2	518 (514)	1920	1920 (1878)
WG8F	491 (488)	1962	1967 (1920)
	497 (494)	1942	
YB10F	507 (504)	1942	1940 (1893)
	522 (518)	1926	1920 (1878)
YCD1F	505 (500)	1943	1942 (1900)
YB10F-WG8F	493 (490)	1966	
	511 (506)	1936	1933 (1890)
YCD1F-WG8F	488 (485)	1967	1967 (1920)
	498 (493)	1952	
YB10F-YCD1F	511 (507)	1931	1933 (1888)
YB10F-YCD1F-WG8F	494 (491)	1955	1957 (1911)

[a]The frequencies of the ^{13}CO complexes are given in parentheses.

(*ii*) *Singly Mutated Variants*. Upon mutation of TrpG8 to Phe, the vibrational spectra are dramatically changed. Two v(FeC) bands are observed at 491 and 497 cm^{-1} and two v(CO) bands at 1962 and 1942 cm^{-1}, the intensity of the 497 and 1942 cm^{-1} bands being much weaker. In fact, the 497 cm^{-1} v(FeC) frequency can be obtained only by a band shape analysis based on a fitting procedure (Figure S4 of the Supporting Information).

Mutation of the distal tyrosines produces very different effects. In fact, only minor changes are observed upon mutation of TyrB10 to Phe. Two v(FeC) bands appear at 507 and 522 cm^{-1} and two v(CO) bands at 1942 and 1926 cm^{-1}. The intensity ratio is very similar to that of the ASV. On the other hand, the YCD1F mutant is characterized by a single v(FeC) band at 505 cm^{-1} and a corresponding v(CO) band at 1943 cm^{-1}.

(*iii*) *Doubly Mutated Variants*. The YB10F-YCD1F variant, in which both distal Tyr residues are missing, shows only one conformer with a v(FeC) band at 511 cm^{-1} and a v(CO) stretching band at 1931 cm^{-1}. Both YB10F-WG8F and YCD1F-WG8F exhibit the presence of two conformers. The RR spectrum of the YB10F-WG8F variant has a major v(FeC) stretching band at 493 cm^{-1} and a weaker one at 511 cm^{-1}. The corresponding v(CO) stretching bands are observed at 1936 and 1966 cm^{-1}, respectively. In the YCD1F-WG8F variant, the v(FeC) bands are observed at 488 and 498 cm^{-1} and the corresponding v(CO) bands at 1967 and 1952 cm^{-1}.

(*iv*) *Triply Mutated Variant*. Only one form is observed with a v(FeC) band at 494 cm^{-1} and a v(CO) band at 1955 cm^{-1} for the YB10F-YCD1F-WG8F triple mutant.

Table 1 lists the v(FeC) and v(CO) vibrational frequencies. The v(FeC) frequencies are obtained by a band shape analysis of the RR spectra of both ^{12}CO and ^{13}CO complexes (Figures S4 and S5 of the Supporting Information).

Molecular Dynamics Simulations. We performed 50 ns MD simulations of Tf-trHb with coordinated CO. We simulated the WT and ASV protein, as well as the YB10F mutant. All three structures were stable during the time scale of the simulation (Figure S6 of the Supporting Information). The mutated residues (Phe107 → Glu and Arg91 → Glu) remained solvent-exposed in both WT and ASV, showing that these mutations do not alter the structure of the protein (Figure S7 of the Supporting Information). We found that TrpG8 is the main residue stabilizing the coordinated CO in both proteins. During the time scale of the
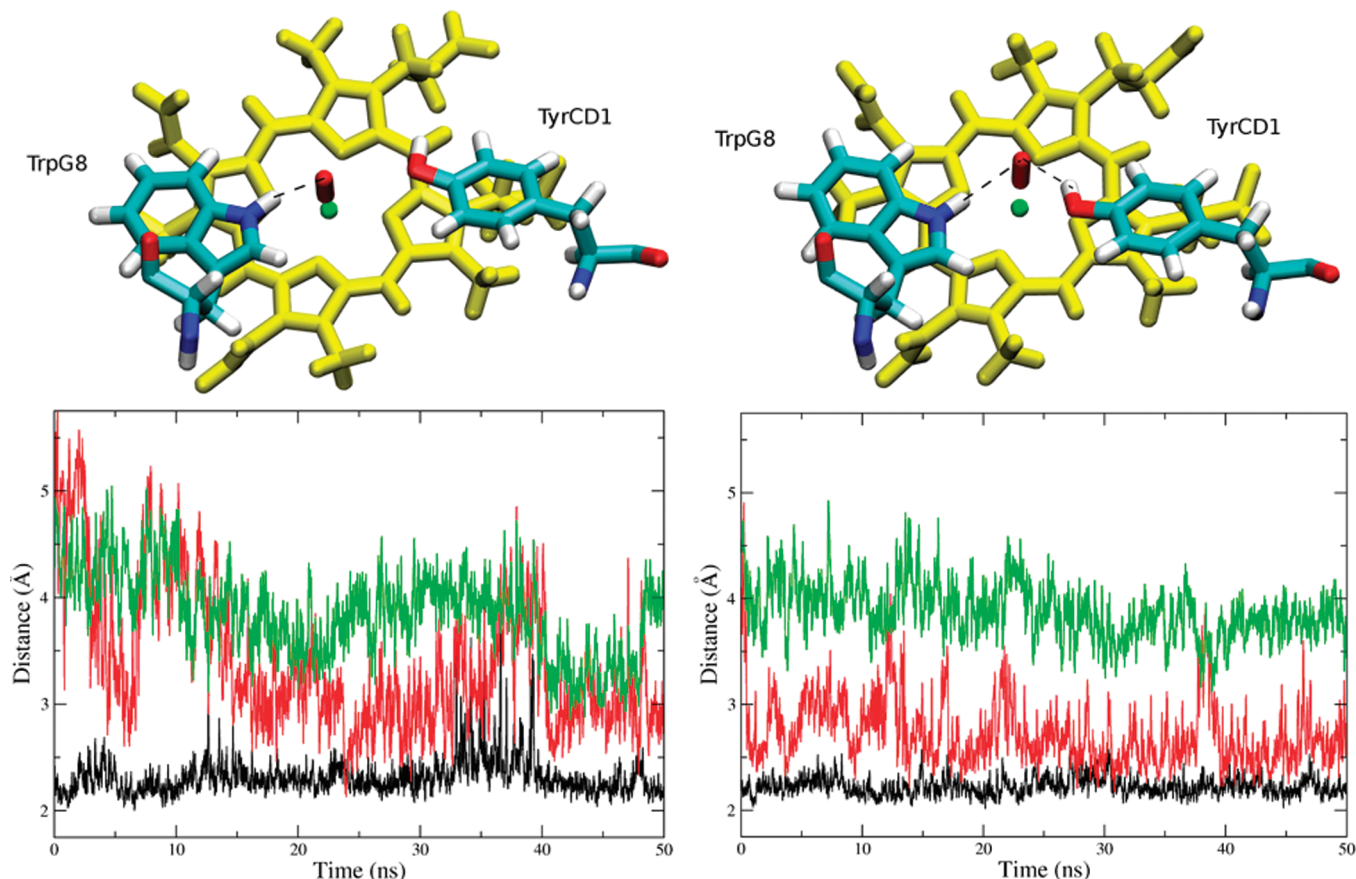
FIGURE 4: Schematic representation of the distal side of Tf-trHb, showing the H-bonds involving the iron-bound CO on the basis of MD simulations (top). Time evolution of selected hydrogen bond distances among the H atom of TrpG8 N_ε (black), the hydroxylic H of TyrCD1 (red), and the hydroxylic H of TyrB10 (green) with the O atom of the coordinated CO (bottom). Data for the WT protein (left) and ASV (right) are shown.

simulation, however, TyrCD1 can move and interact with the coordinated CO, in a conformation in which both TrpG8 and TyrCD1 are involved in the stabilization of the coordinated CO (Figure 4).

The latter residues are also involved in the CO stabilization in the YB10F mutant. TrpG8 forms a strong H-bond with CO, whereas TyrCD1 interacts weakly. However, the TyrCD1 residues in the mutant and in the WT protein behave in different manners (Figure 5). In the WT protein, TyrCD1 forms H-bonds alternatively with CO or with the TyrB10 hydroxyl group. Thus, the distance between the O atoms of the TyrCD1 hydroxyl and CO fluctuates between 2 and 4−5 Å when the H-bond is formed with CO and TyrB10, respectively. In the YB10F mutant, because of the absence of the side chain interactions of TyrB10, TyrCD1 can move far from CO (Figure 5). These results indicate that the TyrB10 residue, though it plays a role in keeping the TyrCD1 close to the active site, does not directly interact with CO.

In the MD simulation of the WT protein, an interesting interaction with the solvent was observed. A water molecule enters the active site via the propionyl gate (the "E7 gate") and remains in intimate contact with TyrB10 near the E7 position (Figure 6). This water molecule does leave the active site and return to the solvent, but another water molecule enters and takes its place. Only one water molecule remains in the active site of the protein at any given time. Accordingly, a H-bonding network involving the heme 7-propionyl group, two water molecules (15 and 64), and TyrB10 is displayed by the X-ray crystal structure.
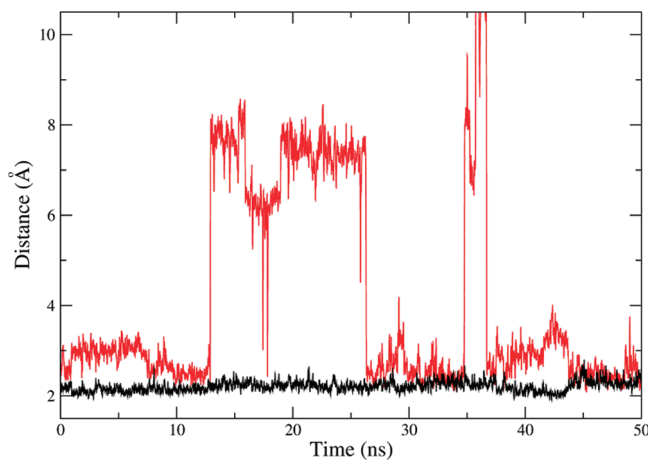

FIGURE 5: Time evolution of selected hydrogen bond distances among H atoms of TrpG8 N_ε (black) and the hydroxylic H of TyrCD1 (red) with the O atom of the coordinated CO, on the basis of MD simulations for the YB10F variant.

DISCUSSION

Ferrous Forms. The RR spectra of ferrous WT Tf-trHb share many characteristics with those of other group II bacterial trHb's, namely, the effects of heme distortion, the weak intensity of the propionyl bending bands, and the frequency of the ν(Fe−Im) stretching mode.

The activation of out-of-plane modes has been reported previously for Mt-trHbO (*30*), and it has been ascribed to distortions
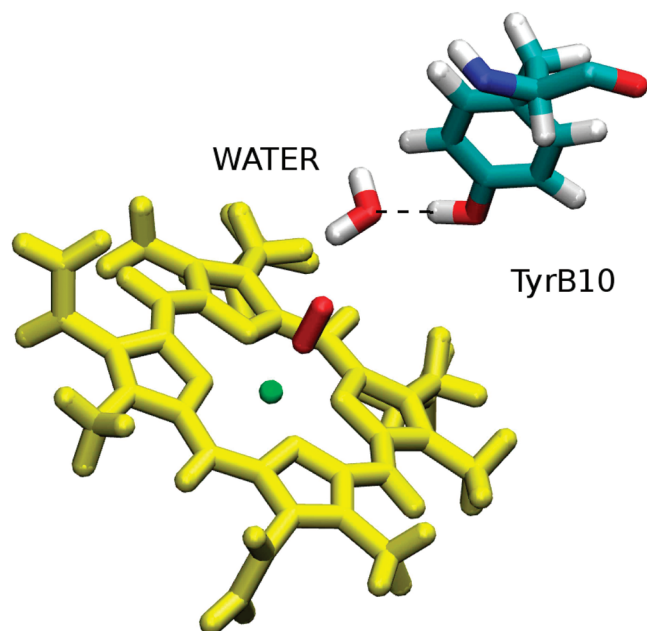
FIGURE 6: Schematic representation of the distal side of Tf-trHb, showing TyrB10 interacting with a water molecule in MD simulations.
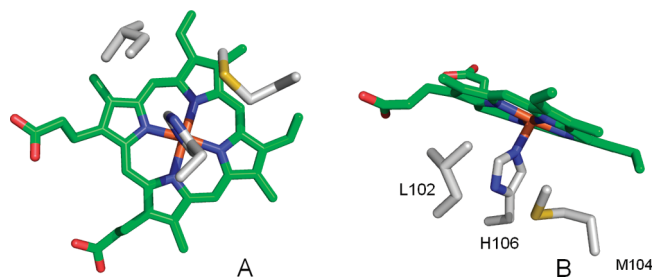

FIGURE 7: Close-up view of the proximal side of Tf-trHb. The proximal histidine (His106) is shown in its relationships with the heme plane (A) and nearby amino acids (Leu102 and Met104). Data from PDB entry 2BMM. The picture was created with Pymol (DeLano Scientific).

of the heme from planarity. This kind of distortion is a consequence of the strain induced on the relatively rigid heme tetrapyrrole ring by the interaction with the protein matrix. Noticeably, the activation of the γ_6 mode is a common feature of both Mt-trHbO and Tf-trHb but is not observed for class I Mt-trHbN.

The weak intensity of the propionyl bending bands is another spectral feature that is shared by both Tf-trHb and Mt-trHbO, at variance with Mt-trHbN. A recent RR study (*31*) has provided evidence of a relationship between the intensity of this band and the orientation of the heme in myoglobin. In fact, the propionyl band is relatively strong in the stable conformation of myoglobin, being the most intense band in the $250-500$ cm^{-1} range. In the unstable conformation, where the heme group is "reversed", i.e., rotated by 180° around the α,γ-meso axis, the propionyl band becomes weaker than the vinyl bending and the ν_8 stretching bands. These findings are in agreement with previous work demonstrating a diminished propionyl band intensity in reconstituted myoglobins in which the substitution of protoporphyrin IX with "symmetric" protoporphyrins also leads to heme reversal (*32*). We note that a structural difference between Mt-trHbN on one side and Mt-trHbO and Tf-trHb on the other is the opposite orientation of the heme group with respect to the α,γ-meso axis (*30*). It is possible, then, that the intensity of the propionyl bending band can be assumed to be a fingerprint of the heme orientation, at least for structurally related proteins.

The frequency of the ν(Fe−His) mode at 223 cm^{-1} is intermediate between that of sperm whale myoglobin (220 cm^{-1}) and those of Mt-trHbO and HbN (226 cm^{-1}). Like those of the latter proteins, the relatively short Fe−His bond can be ascribed to the staggered orientation of the imidazole plane of the proximal His with respect to the heme nitrogen atoms, in contrast to the eclipsed orientation in myoglobin and human adult hemoglobin (*30*). The higher frequency of the Fe−His stretching modes, thus, could in part be a consequence of the weakening of the repulsive interactions between heme and the proximal His, which would allow a stronger Fe coordination. These concepts can be also discussed in structural terms, by taking into account the fact

that the only available X-ray structure (PDB entry 2BMM) involves the ferric, acetate-bound derivative (*6*). In Tf-trHb, the imidazole ring of His106(F8) is comprised of residues Tyr109 and Met104 and the peptide bond of Leu102 (Figure 7A). None of these residues appears to interact directly with HisF8; they simply delimit an apolar cavity in which the imidazole ring is almost rotamerically free with the exception of a small angle in which full rotation is hindered by the sulfur atom of Met104. Accordingly, via inspection of the position of the imidazole plane with respect to the porphyrin nitrogen plane (Figure 7B), it is apparent that the imidazole plane itself is in a fully staggered (with respect to N_p pyrrole atoms) and hence relaxed position. Thus, it might be suggested that the overall architecture of the proximal site in Tf-trHb is such that the Fe−His bond is free of constraint and is able to reach maximal bonding overlap. The suggestion is further supported by recent EXAFS measurements of the ferrous deoxygenated derivative that indicate an unusually compact iron coordination shell, most likely because of the very short length (1.91 Å) of the iron−histidine bond (*33*).

In conclusion, the RR spectra of the ferrous forms are typical of a class II bacterial hemoglobin. Mutations on the distal side of the cavity do not influence the heme distortion or the strength of the proximal His−Fe coordination bond, suggesting that the distal and proximal sides are not coupled for these proteins, as, for example, in peroxidases (*34*).

Carbon Monoxide Complexes. In contrast with the results obtained for the ferrous unbound forms, the spectra of the CO complexes are extremely sensitive to the distal mutations. It is well-known that CO is an excellent probe for investigating the distal cavity of heme proteins (*13*), because back-donation from the Fe d$_\pi$ to the CO π^* orbitals is modulated by polar interactions and, in particular, by the formation of H-bonds between the bound CO and the distal protein residues. The electrostatic field generated by the polar distal pocket amino acids alters the electron distribution in the FeCO unit, changing the order of the C−O bond. A positively charged electrostatic field favors back-donation, which strengthens the Fe−C bond and correspondingly weakens the C−O bond, thereby increasing the ν(FeC) vibrational frequencies and decreasing the ν(CO) frequencies. Conversely, a negatively charged electrostatic field inhibits back-bonding and thus has the opposite effect (*35*). A linear correlation with negative slope between the frequencies of the ν(FeC) and ν(CO) stretching modes has been found for a large class of CO complexes of heme proteins, including bacterial trHb's, and heme model compounds containing imidazole as the fifth iron ligand. The ν(FeC)/ν(CO) position along the correlation line reflects the type and strength of distal polar interactions (*29*).
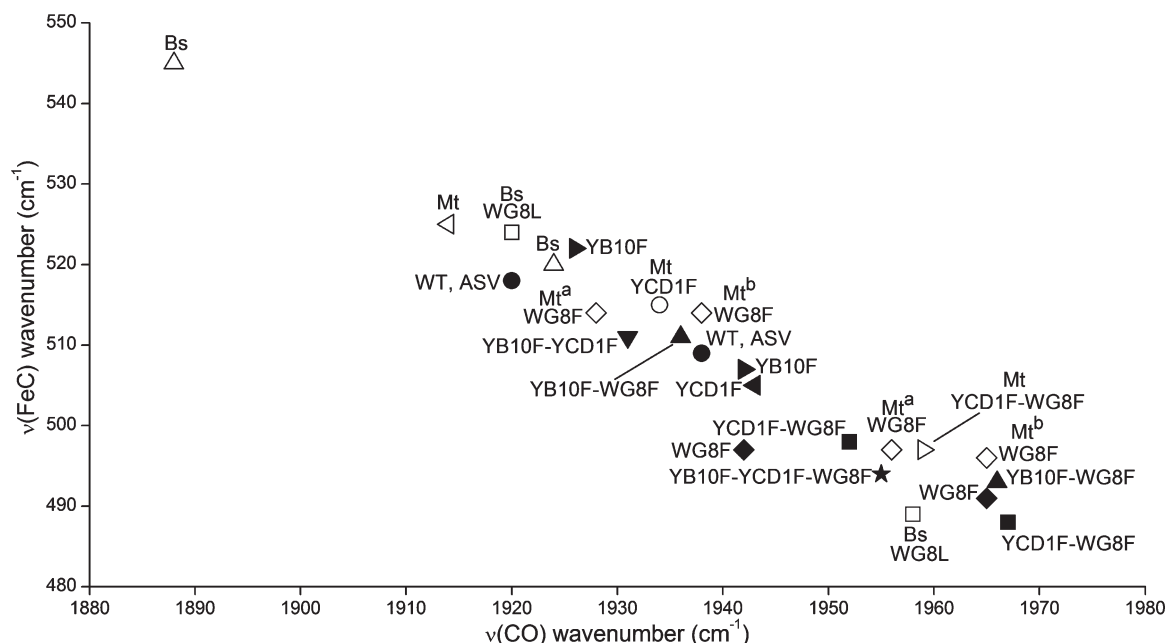
FIGURE 8: Correlation plot between $\nu(FeC)$ and $\nu(CO)$ frequencies of the following proteins: Bs-trHb and its TrpG8-Leu mutant (*11*); Mt-trHbO (*39, 40*) and its WG8F mutant, as measured by different authors [a (*41*) and b (*40*)], its YCD1F mutant (*39*), and its YCD1-WG8F mutant (*41*); and Tf-trHb WT and ASV and its WG8F, YB10F, YCD1F, YB10F-WG8F, YCD1F-WG8F, YB10F-YCD1F, and YB10F-YCD1F-WG8F mutants (this work).

Figure 8 shows a plot of $\nu(FeC)$ versus $\nu(CO)$ frequencies of the Tf-trHb−CO complexes, together with literature data. WT and the ASV are characterized by two conformers: form 1 with $\nu(FeC)$ and $\nu(CO)$ at 509 and 1938 cm^{-1}, respectively, and form 2 with $\nu(FeC)$ and $\nu(CO)$ at 518 and 1920 cm^{-1}, respectively. Both conformers reside in the center of the plot, indicating that the bound CO is stabilized by polar interactions. In a first simplified scheme, we assume that CO interacts with a single H-bond donor in form 1, whereas form 2 is stabilized by two H-bonds. We then consider the crystal structure of ferric, acetate-bound Tf-trHb (Figure 1). The carboxyl carbon atom of the acetate ligand, which can be approximately viewed as the analogue of the oxygen atom of bound CO, is close to both the hydroxyl oxygen of TyrCD1 (3.65 Å) and the indole N atom of TrpG8 (3.36 Å). The hydroxyl oxygen of TyrB10 is slightly more distant (4.04 Å). Therefore, a conclusive view of the molecular interactions giving rise to multiple conformers requires both an analysis of the spectral data for all the distal mutants and the aid of MD. The MD simulation shows that, during the time scale of the simulation, TrpG8 is bound to the coordinated CO. Otherwise, TyrCD1 is very flexible and can interact with CO more weakly than TrpG8. These results suggest that the less polar form 1 corresponds to the TrpG8 residue H-bonded to CO, and the more polar form 2 corresponds to TrpG8 and TyrCD1 both H-bonded to the coordinated CO.

The relevant role of H-bonding between CO and TrpG8 in the stabilization of both forms 1 and 2 is highlighted by the spectra of the WG8F mutant. In fact, this is the only single mutation giving rise to FeCO vibrational frequencies consistent with conformers with absent [$\nu(FeC)$ and $\nu(CO)$ at 491 and 1962 cm^{-1}, respectively] or weak [$\nu(FeC)$ and $\nu(CO)$ at 497 and 1942 cm^{-1}, respectively] polar interactions with the surrounding amino acids. Using the same line of reasoning, the role of TrpG8 is confirmed by the spectra of the double mutant YCD1F-YB10F, which displays a fairly strong CO−Trp polar interaction [$\nu(FeC)$ and $\nu(CO)$ at 511 and 1931 cm^{-1}, respectively].

The spectra of the single mutants YCD1F and YB10F confirm the assignment of forms 1 and 2 to a single CO−TrpG8 interaction and a double CO−TrpG8/CO−TyrCD1 interaction, respectively. On the plot in Figure 8, both YB10F points fall very close to the corresponding points of WT and the ASV. This suggests that, apart from a minor effect of the mutation, CO is surrounded by an environment similar to that of the native protein. On the other hand, a very strong effect is exerted by the YCD1 mutation, because only one conformer (the less polar one) survives in YCD1F. Both results are in agreement with the picture drawn on the basis of MD simulations.

The double mutants in which TrpG8 and either Tyr are mutated show a fairly distinct behavior. The double variant YCD1F-WG8F behaves like the WG8F single mutant, being characterized by two conformers, displaying no [$\nu(FeC)$ and $\nu(CO)$ at 488 and 1967 cm^{-1}, respectively] or very weak [$\nu(FeC)$ and $\nu(CO)$ at 498 and 1952 cm^{-1}, respectively] polar interactions with the surrounding amino acids. The YB10F-WG8F mutant has one form [$\nu(FeC)$ at 493 cm^{-1} and $\nu(CO)$ at 1966 cm^{-1}] characterized by very weak polar interactions, but also a second one [$\nu(FeC)$ at 511 cm^{-1} and $\nu(CO)$ at 1936 cm^{-1}] that experiences a polar environment, deriving from a H-bonding interaction with the TyrCD1 residue. These findings are consistent with the single mutant results and again point to a minor role of TyrB10 in the CO−distal pocket interactions.

As expected, only one apolar form [$\nu(FeC)$ at 494 cm^{-1} and $\nu(CO)$ at 1955 cm^{-1}] is observed in the case of the triple Phe mutation. The frequencies of this form are not at the extreme right of the plot, like those observed for those mutants in which YB10 has not been mutated [WG8F with $\nu(FeC)$ and $\nu(CO)$ at 491 and 1965 cm^{-1}, respectively, and YCD1F-WG8F with $\nu(FeC)$ and $\nu(CO)$ at 488 and 1967 cm^{-1}, respectively]. A tentative explanation is that the nonbonding lone pairs of the TyrB10 hydroxyl group, when this residue is present in the cavity, are oriented toward the CO ligand, providing negative polarity and weakened backbonding from Fe to CO (*36*). As a consequence, the substitution of

TyrB10 with Phe would suppress this negative contribution and restore a moderately positive polar environment.

Comparison with Other Heme Proteins. This spectroscopic and computational characterization indicates that the polar distal residues form a H-bonding network, in which the bound ligand can either interact with the Trp residue alone (form 1) or be caged by Trp and the distal Tyr couple, where TyrCD1 has a prevalent role (form 2). It is useful first to compare the presence of these forms with similar yet not identical observations that have been made with other class II trHb's, namely, Mt-trHbO and Bs-trHb.

The CO complex of Mt-trHbO displays only one conformer [ν(FeC) and ν(CO) at 525 and 1918 cm^{-1}, respectively] (*37*). The combination of RR spectroscopy, mutagenesis, and MD has allowed the conclusion that the heme-bound CO mainly interacts with TrpG8 and TyrCD1 (*38, 39*) in this single conformer to be made, also in agreement with the crystal structure of CN-bound Mt-trHbO, where cyanide is H-bonded to these residues (*40*). These results, however, indicate that the distal interactions in Mt-trHbO and Tf-trHb are different, in spite of the occurrence of the Trp-Tyr-Tyr triad in both proteins. The structural difference could be identified with an increased mobility of the distal Tyr residues in Tf-trHb, leading to the appearance of form 1, which is singly H-bonded with TrpG8.

The comparison with Bs-trHb shows even more striking differences, which can be expected on the basis of the distal cavity structure, which is bordered by the polar amino acids TrpG8, TyrB10, and GlnE11. The case of the CO complexes of Bs-trHb can be considered as an extreme one, because the effect of back-bonding on the FeCO vibrational frequencies is one of the strongest observed. In fact, two conformers are observed, the more polar of which displays ν(FeC) and ν(CO) at 545 and 1888 cm^{-1}, respectively. Thus, it is confirmed that the polarity of the distal cavity in Bs-trHb is unique among bacterial hemoglobins.

These observations allow us to conclude that the polarity of the Tf-trHb distal cavity is intermediate between that of vertebrate hemoglobins and that of heme-containing peroxidases. In particular, the FeCO frequencies of form 2 are reminiscent of a peroxidase-like conformer: *Coprinus cinereus* peroxidase [CIP, ν(FeC) and ν(CO) at 519 and 1930 cm^{-1}, respectively] (*41*), form 2 of horseradish peroxidase [HRP, ν(FeC) and ν(CO) at 516 and 1933 cm^{-1}, respectively] (*42, 43*), and form 2 of cytochrome *c* peroxidase [CCP, ν(FeC) and ν(CO) at 530 and 1922 cm^{-1}, respectively] (*44*). This spectral correlation is consistent with recent findings of the genuine peroxidase activity possessed by Tf-trHb (*45*). Tf-trHb peroxidase activity is common to other bacterial truncated hemoglobins, such as Mt-trHbO (*46*). On the other hand, it must be considered that the similar polarity of the distal cavities of trHb's and peroxidases stems from amino acids with very different structural and acid−base properties. In particular, peroxidases possess positively charged residues, like His and Arg, that are able to polarize the hydrogen peroxide ligand. The possibility that the Trp-Tyr pair may mimic the His-Arg couple is consistent with the previously observed decrease in the peroxidase activity in the Trp-Phe mutants (*45*). Nevertheless, the details of the molecular mechanism of the reactions catalyzed by trHb's will need to be studied further.

SUPPORTING INFORMATION AVAILABLE

SDS−PAGE of WT and the ASV, electronic absorption spectra of ferrous forms, RR spectra in the ν(CO) region of ^{12}CO and ^{13}CO complexes, ν(FeC) band fitting analysis of ^{12}CO and ^{13}CO complexes, structure stability during the MD simulations, and the solvent environment of the mutated residues in the ASV. This material is available free of charge via the Internet at http://pubs.acs.org.

REFERENCES

1. Wittenberg, J. B., Bolognesi, M., Wittenberg, B. A., and Guertin, M. (2002) Truncated hemoglobins: A new family of hemoglobins widely distributed in bacteria, unicellular eukaryotes, and plants. *J. Biol. Chem. 277*, 871–874.
2. Wu, G., Wainwright, L. M., and Poole, R. K. (2003) Microbial globins. *Adv. Microb. Physiol. 47*, 255–310.
3. Milani, M., Pesce, A., Nardini, M., Ouellet, H., Ouellet, Y., Dewilde, S., Bocedi, A., Ascenzi, P., Guertin, M., Moens, L., Friedman, J. M., Wittenberg, J. B., and Bolognesi, M. (2005) Structural bases for heme binding and diatomic ligand recognition in truncated hemoglobins. *J. Inorg. Biochem. 99*, 97–109.
4. Vuletich, D. A., and Lecomte, J. T. (2006) A phylogenetic and structural analysis of truncated hemoglobins. *J. Mol. Evol. 62*, 196–210.
5. Giangiacomo, L., Ilari, A., Boffi, A., Morea, V., and Chiancone, E. (2005) The truncated oxygen-avid hemoglobin from *Bacillus subtilis*: X-ray structure and ligand binding properties. *J. Biol. Chem. 280*, 9192–9202.
6. Bonamore, A., Ilari, A., Giangiacomo, L., Bellelli, A., Morea, V., and Boffi, A. (2005) A novel thermostable hemoglobin from the actino-bacterium *Thermobifida fusca*. *FEBS J. 272*, 4189–4201.
7. Ilari, A., Kjelgaard, P., von Wachenfeldt, C., Catacchio, B., Chiancone, E., and Boffi, A. (2007) Crystal structure and ligand binding properties of the truncated hemoglobin from *Geobacillus stearothermophilus*. *Arch. Biochem. Biophys. 457*, 85–94.
8. Milani, M., Savard, P. Y., Ouellet, H., Ascenzi, P., Guertin, M., and Bolognesi, M. (2003) A TyrCD1/TrpG8 hydrogen bond network and a TyrB10TyrCD1 covalent link shape the heme distal site of *Mycobacterium tuberculosis* hemoglobin O. *Proc. Natl. Acad. Sci. U.S.A. 100*, 5766–5771.
9. Ouellet, H., Juszczak, L., Dantsker, D., Samuni, U., Ouellet, Y. H., Savard, P. Y., Wittenberg, J. B., Wittenberg, B. A., Friedman, J. M., and Guertin, M. (2003) Reactions of *Mycobacterium tuberculosis* truncated hemoglobin O with ligands reveal a novel ligand-inclusive hydrogen bond network. *Biochemistry 42*, 5764–5774.
10. Boechi, L., Manez, P. A., Luque, F. J., Marti, M. A., and Estrin, D. A. (2010) Unraveling the molecular basis for ligand binding in truncated hemoglobins: The trHbO *Bacillus subtilis* case. *Proteins 78*, 962–970.
11. Feis, A., Lapini, A., Catacchio, B., Brogioni, S., Foggi, P., Chiancone, E., Boffi, A., and Smulevich, G. (2008) Unusually strong H-bonding to the heme ligand and fast geminate recombination dynamics of the carbon monoxide complex of *Bacillus subtilis* truncated hemoglobin. *Biochemistry 47*, 902–910.
12. Lu, C., Egawa, T., Mukai, M., Poole, R. K., and Yeh, S. R. (2008) Hemoglobins from *Mycobacterium tuberculosis* and *Campylobacter jejuni*: A comparative study with resonance Raman spectroscopy. *Methods Enzymol. 437*, 255–286.
13. Spiro, T. G., and Wasbotten, I. H. (2005) CO as a vibrational probe of heme protein active sites. *J. Inorg. Biochem. 99*, 34–44.
14. Arroyo-Manez, P., Bikiel, D. E., Boechi, L., Capece, L., Di Lella, S., Estrin, D. A., Marti, M. A., Moreno, D. M., Nadra, A. D., and Petruk, A. A. (2010) Protein dynamics and ligand migration interplay as studied by computer simulation. *Biochim. Biophys. Acta* (in press).
15. Bidon-Chanal, A., Marti, M. A., Estrin, D. A., and Luque, F. J. (2007) Dynamical regulation of ligand migration by a gate-opening molecular switch in truncated hemoglobin-N from *Mycobacterium tuberculosis*. *J. Am. Chem. Soc. 129*, 6782–6788.
16. Boechi, L., Marti, M. A., Milani, M., Bolognesi, M., Luque, F. J., and Estrin, D. A. (2008) Structural determinants of ligand migration in *Mycobacterium tuberculosis* truncated hemoglobin O. *Proteins 73*, 372–379.
17. Marti, M. A., Bikiel, D. E., Crespo, A., Nardini, M., Bolognesi, M., and Estrin, D. A. (2006) Two distinct heme distal site states define *Cerebratulus lacteus* mini-hemoglobin oxygen affinity. *Proteins 62*, 641–648.
18. Marti, M. A., Capece, L., Bikiel, D. E., Falcone, B., and Estrin, D. A. (2007) Oxygen affinity controlled by dynamical distal conformations: The soybean leghemoglobin and the *Paramecium caudatum* hemoglobin cases. *Proteins 68*, 480–487.

19. Nicoletti, F. P., Comandini, A., Bonamore, A., Boechi, L., Boubeta, F. M., Feis, A., Smulevich, G., and Boffi, A. (2010) Sulfide Binding Properties of Truncated Hemoglobins. *Biochemistry 49*, 2269–2278.

20. Jorgensen, W. L., Chandrasekar, J., Madura, J., Impey, R. W., and Klein, M. L. (1983) Comparison of simple potential functions for simulating liquid water. *J. Chem. Phys. 79*, 926–935.

21. Ryckaert, J. P., Ciccoti, G., and Berendsen, H. J. C. (1977) Numerical integration of the Cartesian equations of motion of a system with constraints: Molecular dynamics of n-alkanes. *J. Comput. Phys. 23*, 327–341.

22. Pearlman, D. A., Case, D. A., Caldwell, J. W., Ross, W. S., Cheatham, T. E., Debolt, S., Ferguson, D., Seibel, G., and Kollman, P. (1995) AMBER, a package of computer programs for applying molecular mechanics, normal mode analysis, molecular dynamics and free energy calculations to simulate the structural and energetic properties of molecules. *Comput. Phys. Commun. 91*, 1–41.

23. Hori, H., and Kitagawa, T. (1980) Iron-ligand stretching band in the resonance Raman spectra of ferrous iron porphyrin derivatives. Importance as a probe band for quaternary structure of hemoglobin. *J. Am. Chem. Soc. 102*, 3608–3613.

24. Spiro, T. G., and Li, X.-Y. (1988) in Biological Application of Raman Spectroscopy (Spiro, T. G., Ed.) Vol. 3, pp 1–37, Wiley-Interscience, New York.

25. Stein, P., and Spiro, T. G. (1980) Hydrogen-bond and deprotonation effects on the resonance Raman iron-imidazole mode in deoxy hemoglobin models: Implication for hemoglobin cooperativity. *J. Am. Chem. Soc. 102*, 7795–7797.

26. Blackwood, M. E., Jr., Rush, T. S., III, Romesberg, F., Schultz, P. G., and Spiro, T. G. (1998) Alternative modes of substrate distortion in enzyme and antibody catalyzed ferrochelation reactions. *Biochemistry 37*, 779–782.

27. Hu, S., Smith, K. M., and Spiro, T. G. (1996) Assignment of Protoheme Resonance Raman Spectrum by Heme Labeling in Myoglobin. *J. Am. Chem. Soc. 118*, 12638–12646.

28. Smulevich, G., Hu, S. Z., Rodgers, K. R., Goodin, D. B., Smith, K. M., and Spiro, T. G. (1996) Heme-protein interactions in cytochrome c peroxidase revealed by site-directed mutagenesis and resonance Raman spectra of isotopically labeled hemes. *Biospectroscopy 2*, 365–376.

29. Egawa, T., and Yeh, S. R. (2005) Structural and functional properties of hemoglobins from unicellular organisms as revealed by resonance Raman spectroscopy. *J. Inorg. Biochem. 99*, 72–96.

30. Samuni, U., Ouellet, Y., Guertin, M., Friedman, J. M., and Yeh, S. R. (2004) The absence of proximal strain in the truncated hemoglobins from *Mycobacterium tuberculosis. J. Am. Chem. Soc. 126*, 2682–2683.

31. Rwere, F., Mak, P. J., and Kincaid, J. R. (2008) Resonance Raman interrogation of the consequences of heme rotational disorder in myoglobin and its ligated derivatives. *Biochemistry 47*, 12869–12877.

32. Mie, Y., Yamada, C., Hareau, G. P., Neya, S., Uno, T., Funasaki, N., Nishiyama, K., and Taniguchi, I. (2004) Functional evaluation of heme vinyl groups in myoglobin with symmetric protoheme isomers. *Biochemistry 43*, 13149–13155.

33. Arcovito, A., Bonamore, A., Hazemann, J. L., Boffi, A., and D'Angelo, P. (2010) Unusual proximal heme pocket geometry in the deoxygenated *Thermobifida fusca*: A combined spectroscopic investigation. *Biophys. Chem. 147*, 1–7.

34. Smulevich, G., Feis, A., and Howes, B. D. (2005) Fifteen years of Raman spectroscopy of engineered heme containing peroxidases: What have we learned? *Acc. Chem. Res. 38*, 433–440.

35. Phillips, G. N., Jr., Teodoro, M. L., Li, T., Smith, B., and Olson, J. S. (1999) Bound CO Is a Molecular Probe of Electrostatic Potential in the Distal Pocket of Myoglobin. *J. Phys. Chem. B 103*, 8817–8829.

36. Cameron, A. D., Smerdon, S. J., Wilkinson, A. J., Habash, J., Helliwell, J. R., Li, T., and Olson, J. S. (1993) Distal pocket polarity in ligand binding to myoglobin: Deoxy and carbonmonoxy forms of a threonine68(E11) mutant investigated by X-ray crystallography and infrared spectroscopy. *Biochemistry 32*, 13061–13070.

37. Mukai, M., Savard, P. Y., Ouellet, H., Guertin, M., and Yeh, S. R. (2002) Unique ligand-protein interactions in a new truncated hemoglobin from *Mycobacterium tuberculosis. Biochemistry 41*, 3897–3905.

38. Guallar, V., Lu, C., Borrelli, K., Egawa, T., and Yeh, S. R. (2009) Ligand Migration in the Truncated Hemoglobin-II from *Mycobacterium tuberculosis*: The Role of G8 Tryptophan. *J. Biol. Chem. 284*, 3106–3116.

39. Ouellet, H., Milani, M., LaBarre, M., Bolognesi, M., Couture, M., and Guertin, M. (2007) The roles of Tyr(CD1) and Trp(G8) in *Mycobacterium tuberculosis* truncated hemoglobin O in ligand binding and on the heme distal site architecture. *Biochemistry 46*, 11440–11450.

40. Milani, M., Ouellet, Y., Ouellet, H., Guertin, M., Boffi, A., Antonini, G., Bocedi, A., Mattu, M., Bolognesi, M., and Ascenzi, P. (2004) Cyanide binding to truncated hemoglobins: A crystallographic and kinetic study. *Biochemistry 43*, 5213–5221.

41. Feis, A., Santoni, E., Neri, F., Ciaccio, C., De Sanctis, G., Coletta, M., Welinder, K. G., and Smulevich, G. (2002) Fine-tuning of the binding and dissociation of CO by the amino acids of the heme pocket of *Coprinus cinereus* peroxidase. *Biochemistry 41*, 13264–13273.

42. Feis, A., Rodriguez-Lopez, J. N., Thorneley, R. N., and Smulevich, G. (1998) The distal cavity structure of carbonyl horseradish peroxidase as probed by the resonance Raman spectra of His 42 Leu and Arg 38 Leu mutants. *Biochemistry 37*, 13575–13581.

43. Uno, T., Nishimura, Y., Tsuboi, M., Makino, R., Iizuka, T., and Ishimura, Y. (1987) Two types of conformers with distinct Fe-C-O configuration in the ferrous CO complex of horseradish peroxidase. Resonance Raman and infarared spectroscopic studies with native and deuteroheme-substituted enzymes. *J. Biol. Chem. 262*, 4549–4556.

44. Smulevich, G., Evangelista-Kirkup, R., English, A., and Spiro, T. G. (1986) Raman and infrared spectra of cytochrome c peroxidase-carbon monoxide adducts in alternative conformational states. *Biochemistry 25*, 4426–4430.

45. Torge, R., Comandini, A., Catacchio, B., Bonamore, A., Botta, B., and Boffi, A. (2009) Peroxidase-like activity of *Thermobifida fusca* hemoglobin: The oxidation of dibenzylbutanolide. *J. Mol. Catal. B: Enzym. 61*, 303–308.

46. Ouellet, H., Ranguelova, K., Labarre, M., Wittenberg, J. B., Wittenberg, B. A., Magliozzo, R. S., and Guertin, M. (2007) Reaction of *Mycobacterium tuberculosis* truncated hemoglobin O with hydrogen peroxide: Evidence for peroxidatic activity and formation of protein-based radicals. *J. Biol. Chem. 282*, 7491–7503.